Fast Fringe Pattern Phase Demodulation using FIR Hilbert Transformers

Munther Gdeisat[a*], David Burton[b], Francis Lilley[b], Miguel Arevalillo-Herráez[c]

[a*] *Corresponding Author: Colleges of Applied Sciences, Sohar, PO BOX 135, Post Code 311, Oman (e-mail: gdeisat@hotmail.com).*

[b]*The General Engineering Research Institute, Liverpool John Moores University, Liverpool L3 3AF, UK (e-mail: d.r.burton@ljmu.ac.uk, f.lilley@ljmu.ac.uk).*

[c]*Departament d'Informàtica. Universitat de València, 46100. Burjassot, Valencia, Spain (e-mail: miguel.arevalillo@uv.es).*

Abstract

This paper suggests the use of FIR Hilbert transformers to extract the phase of fringe patterns. This method is computationally faster than any known spatial method that produces wrapped phase maps. Also, the algorithm does not require any parameters to be adjusted which are dependent upon the specific fringe pattern that is being processed, or upon the particular setup of the optical fringe projection system that is being used. It is therefore particularly suitable for full algorithmic automation. The accuracy and validity of the suggested method has been tested using both computer-generated and real fringe patterns. This novel algorithm has been proposed for its advantages in terms of computational processing speed as it is the fastest available method to extract the wrapped phase information from a fringe pattern.

Keywords: Phase demodulation, Hilbert transform, fringe pattern, wrapped phase map.

1. Introduction

Many image processing applications exist that require the extraction of the phase of fringe patterns and interferograms [1]. Algorithms to extract the phase information can be classified as a) temporal algorithms that require three, or more, source images; b) and non-temporal (e.g. spatial) algorithms that only require one, or two, source images. An example of the first category is phase stepping [2]. Examples of the latter category are Fourier transform approaches [3], wavelet transform methods [4] and techniques employing complex finite impulse response (FIR) filters [5].

Every algorithm that has been developed for extracting the phase information from a fringe image has its various merits and drawbacks. The phase stepping algorithm is reliable and it produces accurate results, but requires a minimum of three images. This makes it unsuitable for use in measuring dynamic objects. In addition, this technique generally relies on the introduction of highly accurate phase steps. These are usually achieved by mechanical methods and small errors may significantly affect the accuracy of the results. Fourier transform profilometry generally requires only a single source image, but suffers from a number of disadvantages, such as the intrinsic difficulty of separating the effects of the background illumination from the fringe phase information in the frequency domain. Also, the accuracy of this method is affected by leakage effects in the frequency domain, which manifest as distortion at the edges of the resultant phase information images [6]. Regarding wavelet methods, these can be very time consuming. For example, wavelet processing of a fringe pattern image typically requires more than a one-hundred fold increase in processing time in comparison with phase stepping, or Fourier methods [4, 7].

Qian *et al.* [5] proposed the use of complex FIR filters to process fringe patterns in the spatial domain as an alternative to processing them in the frequency domain. However, with their proposed method it was necessary to calibrate system parameters depending upon the specific setup of the fringe projection system. It was also necessary to determine appropriate values for the filter bandwidth and filter center frequency such that they are suitable to process individual fringe patterns. The filter was initially implemented in the frequency domain and then the inverse Fourier transform was used to calculate the coefficients of the complex FIR filter. The coefficients of the complex FIR filter may vary according to the spectrum of the fringe pattern being processed. This significantly complicates the automation of this method as it is necessary to calibrate its parameters depending on both the setup of the fringe projection system being employed and also upon the characteristics of the specific fringe pattern image that is undergoing processing.

This paper suggests the use of real FIR Hilbert transformer filters to extract the phase of a fringe pattern. This method is simple to fully automate because it is not necessary to calibrate any

individual system parameters depending on either the specific source fringe pattern image, or the particular fringe projection system being employed. The proposed method is also very fast in comparison to other phase extraction methods, as will be explained later.

2. The algorithm

A fringe pattern image can be described using the well-known equation [7]

$$g(x,y) = a(x,y) + b(x,y)cos(2\pi f_o x + \emptyset(x,y)) \quad (1)$$

Where $a(x,y)$ represents the background illumination, $b(x,y)$ the amplitude modulation of the fringes, f_o the spatial carrier frequency, $\emptyset(x,y)$ the phase modulation of the fringes and x and y are the sample indices for the x and y axes respectively.

The Hilbert transform can be used to extract the phase in a fringe pattern. The Hilbert transform for a fringe pattern can be also implemented using a discrete Fourier transform as follows. The spectrum of the fringe pattern is calculated using a two-dimensional discrete Fourier transform. The positive part of the spectrum is selected and the negative part is set to zero. The two-dimensional inverse discrete Fourier transform is then calculated. The real part resulting from the application of the inverse discrete Fourier transform is the fringe pattern itself, whereas the imaginary part is a π/2 phase shifted version of the fringe pattern [8].

Rabiner and Schafer [9] developed Finite Impulse Response (FIR) digital filters whose frequency response is an approximation to the frequency response of an ideal Hilbert transformer. The frequency response of the digital filter approaches the frequency response of the ideal Hilbert transformer as the number of elements of the digital filter increases. The coefficients of a 7-element FIR Hilbert transformer are [-0.1270413, 0, -0.6012845, 0, 0.6012845, 0, 0.1270413]; whereas the coefficients of a 15-element FIR Hilbert transformer are [-0.0529897, 0.0, -0.0882059, 0.0, -0.1868274, 0.0, -0.6278288, 0.0, 0.6278288, 0.0, 0.1868274, 0.0, 0.0882059, 0.0, 0.0529897]. The frequency responses of both filters are shown in Fig. 1. The cut-off frequencies of the 7-element digital filter are 0.1 and 0.4. Whereas the cut-off frequencies of the 15-element digital filter are 0.05 and 0.45.

Generally, the implementation of the Hilbert transform using an FIR digital filter is less computationally intensive than the implementation with the aid of the discrete Fourier transform. The 7-element FIR Hilbert transformer is mainly used here to implement the Hilbert transform. When the sampling rate of a fringe pattern is very high (*i.e.* greater than 10 samples per fringe), then the 15-element FIR Hilbert transformer should be used. This is because the cut-off frequency of the 15-element FIR Hilbert transformer is 0.1.

The phase of the fringe pattern $g(x, y)$ can be extracted using the FIR filter approximation of the Hilbert transform, as is shown in Fig. 2. Initially, this FIR filter is used to remove the background illumination of the fringe pattern. The output of this filter is then applied a second time to the FIR Hilbert transformer. After that, the outputs of both filters are applied to the arctangent function to calculate the wrapped phase map.

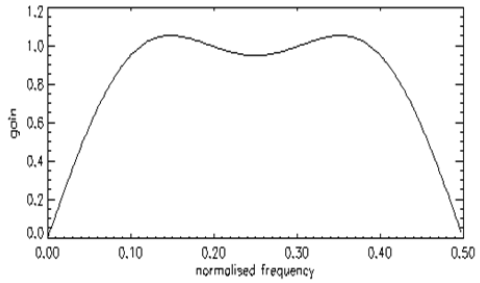

(a)

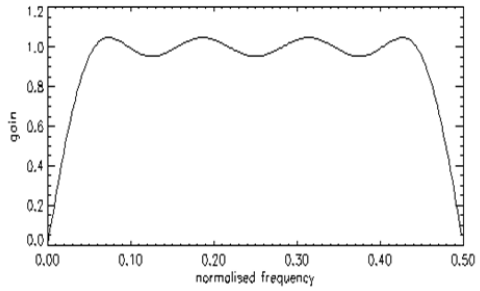

(b)

Figure 1: Frequency response of (a) a 7-element and a (b) 15-element Hilbert transformers.

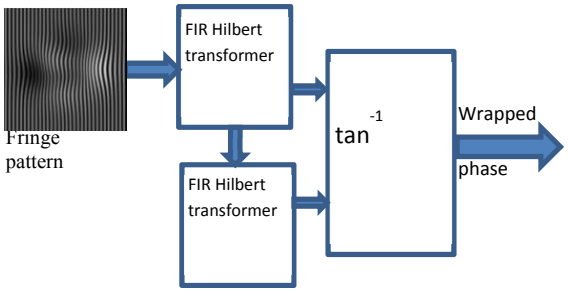

Figure 2: Block diagram of extracting the phase of a fringe pattern using an FIR Hilbert transformer.

3. Simulation Results

Figs. 3(a) and (b) show a computer-generated object that is used to phase modulate fringes. This object consists of 512 × 512 pixels and contains regions with both slowly changing and rapidly changing phase variations. It has become a popular benchmark in the literature for testing the performance of different fringe analysis algorithms [7, 10]. This object can be generated in MATLAB using the *peaks* function and it is shown as an intensity map in Fig. 3a and is also plotted in 3D isometric form in Fig. 3b. The object is given by the equation;

$$\Gamma(x,y) = 3(1-m)^2 e^{-m^2-(n+1)^2} - 10\left(\frac{m}{5} - m^3 - n^5\right) e^{-m^2-n^2} - \frac{1}{3} e^{-(m+1)^2-n^2} + 10 \quad (2)$$

$$m = \frac{3(x-N_x/2)}{N_x/2} \quad (3)$$

$$n = \frac{3(y-N_y/2)}{N_y/2} \quad (4)$$

Where x & y are the sample indices for the x and y axes respectively and both could have a value ranging between 1 and 512. N_x and N_y are the sizes of the image in the x and y directions respectively and both are set here to 512.

The computer-generated object phase modulated fringes according to the equation;

$$g(x,y) = \Gamma(x,y) + \Gamma(x,y)\cos[2\pi f_o x + \beta\Gamma(x,y)] \quad (5)$$

Where f_o is set here to 1/16. The modulation index is set to $\beta = 2$. This parameter depends practically upon the setup of fringe projection system that is used to generate the fringe pattern. The background illumination and amplitude modulation depend on many factors, such as the color, smoothness, and reflection angle of the object. For simplicity, the object is used here as a representation of both functions. The fringe pattern image is shown in Fig. 3c and row 256 of the image is plotted in Fig. 3d.

The fringe pattern is initially applied to the FIR filter on a row-by-row basis and it is filtered using the 15-coefficient version of the FIR Hilbert transformer. The direction of the fringes should run perpendicular to the rows. The resultant wrapped phase map is shown in Fig. 3e. The

wrapped phase is unwrapped using a basic phase unwrapper [11] and the resultant phase is plotted in 3D isometric form as shown in Fig. 3f and also as an intensity map as shown in Fig. 3g.

The arithmetic difference between the computer-generated object and the extracted phase was then calculated and it is plotted in 3D isometric form as shown in Fig. 3h. The standard deviation for this error is 0.001 radians and the maximum value of the error is 0.02265 radians, or approximately ($0.02265/2\pi = 0.0036$) of a fringe. The error is high at the right and left edges of the extracted phase image because of the transient response of the FIR filter. The edges of the resultant image are not cropped here.

The 15-coefficent FIR filter requires eight multiplication operations and seven addition operations to process each pixel. Hence calculating a pixel in the wrapped phase requires 16 multiplication operations and 14 addition operations in addition to calculating the arctangent function. The execution time required to extract the wrapped phase for a fringe pattern with the size of 512 × 512 pixels using the15-coefficent FIR Hilbert transformer was measured using an HP laptop that has 4GRAM and i7 microprocessor and it is found to be 10 msec approximately. This algorithm was programmed using IDL programming language [12].

The above computer simulation was repeated but this time employing the 7-coefficient FIR Hilbert transformer instead of the 15-coefficient version. The resulting wrapped phase map is shown in Fig. 3i. The wrapped phase map was unwrapped using a basic phase unwrapper and the resultant phase is shown as an intensity map in Fig. 3j and it is also plotted in 3D isometric form in Fig. 3k.

The arithmetic difference between the computer-generated object and the extracted phase was calculated and it is plotted in 3D isometric form as shown in Fig. 3l. The standard deviation for this error is 0.0093 radians and the maximum value of the error is 0.026 radians, or approximately ($0.026/2\pi = 0.004$) of a fringe. The 7-coefficent FIR filter requires four multiplication operations and three addition operations to process each pixel. Hence calculating a pixel in the wrapped phase requires 8 multiplication operations and 6 addition operations in

addition to calculating the arctangent function. To the authors' knowledge, this is the fastest spatial phase extraction algorithm in existence.

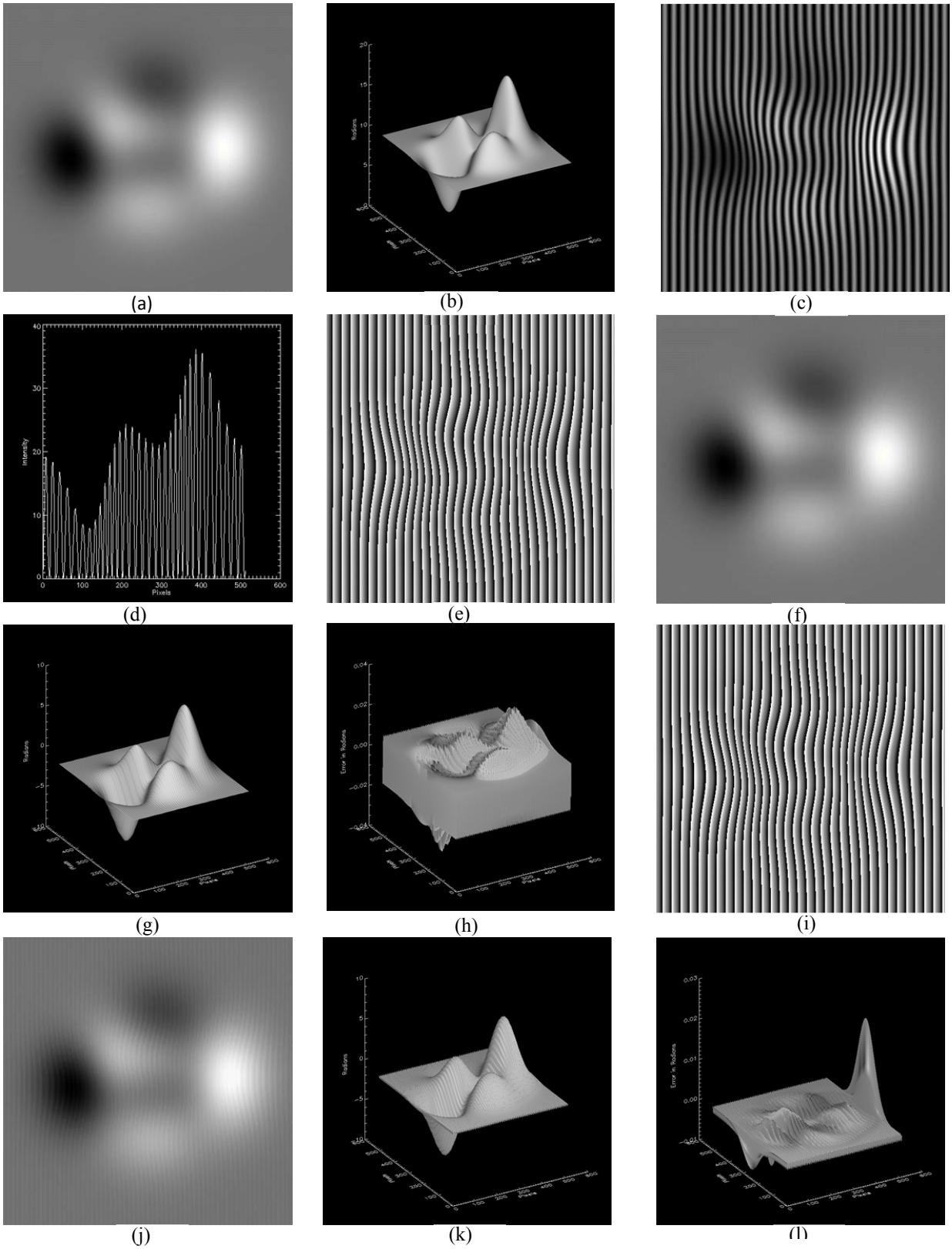

Figure 3: The Process of phase demodulation of a computer-generated fringe pattern using FIR Hilbert transformers.

The error produced by the 15-coefficent FIR Hilbert transformer is related to the modulation index β in Eq. (5). In order to study this relationship, the arithmetic difference between the computer-generated object and the extracted phase was calculated for different values of β varying between 1 and 4. The standard deviations for each of the arithmetic differences were then calculated. The resultant values are shown in Fig. 4a and it shows that the standard deviation of the error starts to increase rapidly when the value of β is larger than 3.5. The value of f_o is set here to 1/16.

The above simulation was repeated but for the spatial carrier frequency f_o. The spatial carrier frequency was varied between 0.05 and 0.11. The resultant standard deviations are plotted in Fig. 4b and show that the lowest error is produced when f_o is equal to 0.08. The parameter β was set here to a value of 2.

The histogram of the arithmetic difference between the computer-generated object and the extracted phase was calculated for the values of $\beta = 2$ and $f_o = 1/16$ and the result is shown in Fig. 4c. The resultant shape for the histogram is very similar to a Gaussian normal distribution function.

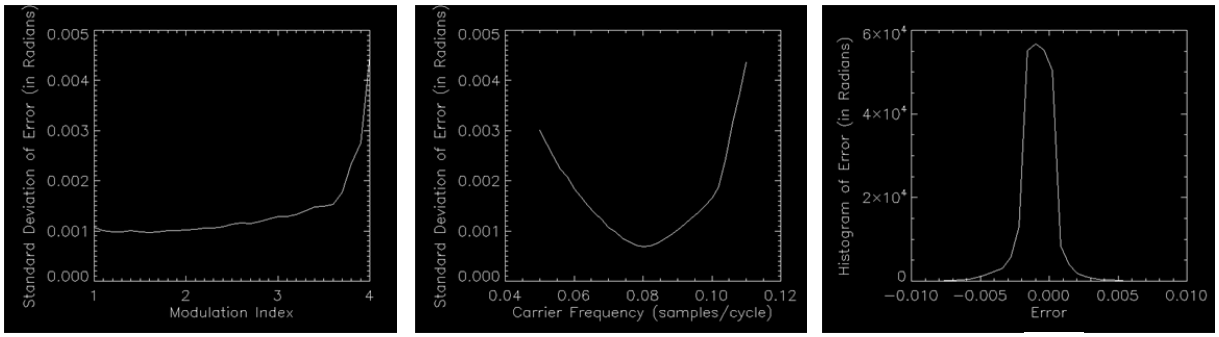

(a) (b) (c)

Figure 4: Errors produced by the 15-coefficient FIR Hilbert transformer.

The fringe pattern shown in Fig. 2c was subsequently also processed using the Fourier transform algorithm for comparison purposes [6]. The resultant wrapped and unwrapped phase maps are shown as 2D intensity images in Figs. 5a and 5b respectively. The unwrapped phase map is also shown as a 3D plot in Fig. 5c. The error produced by the Fourier transform algorithm was computed as the arithmetic difference between the object, shown in Fig. 2b, and the unwrapped phase map, shown in Fig 5c. This error is plotted in 3D in Fig. 5d. The standard deviation of the error is 0.001 radians and the maximum value is 0.025 radians. These values are close to those of the FIR Hilbert transformer method due to the absence of additive noise. The histogram of the error is plotted in 3D in Fig. 5e. The execution time required to extract the wrapped phase for a fringe pattern with the size of 512 × 512 pixels using the Fourier transform method was measured using the HP laptop and it is found to be 90 msec approximately. This algorithm was also programmed using IDL programming language [12].

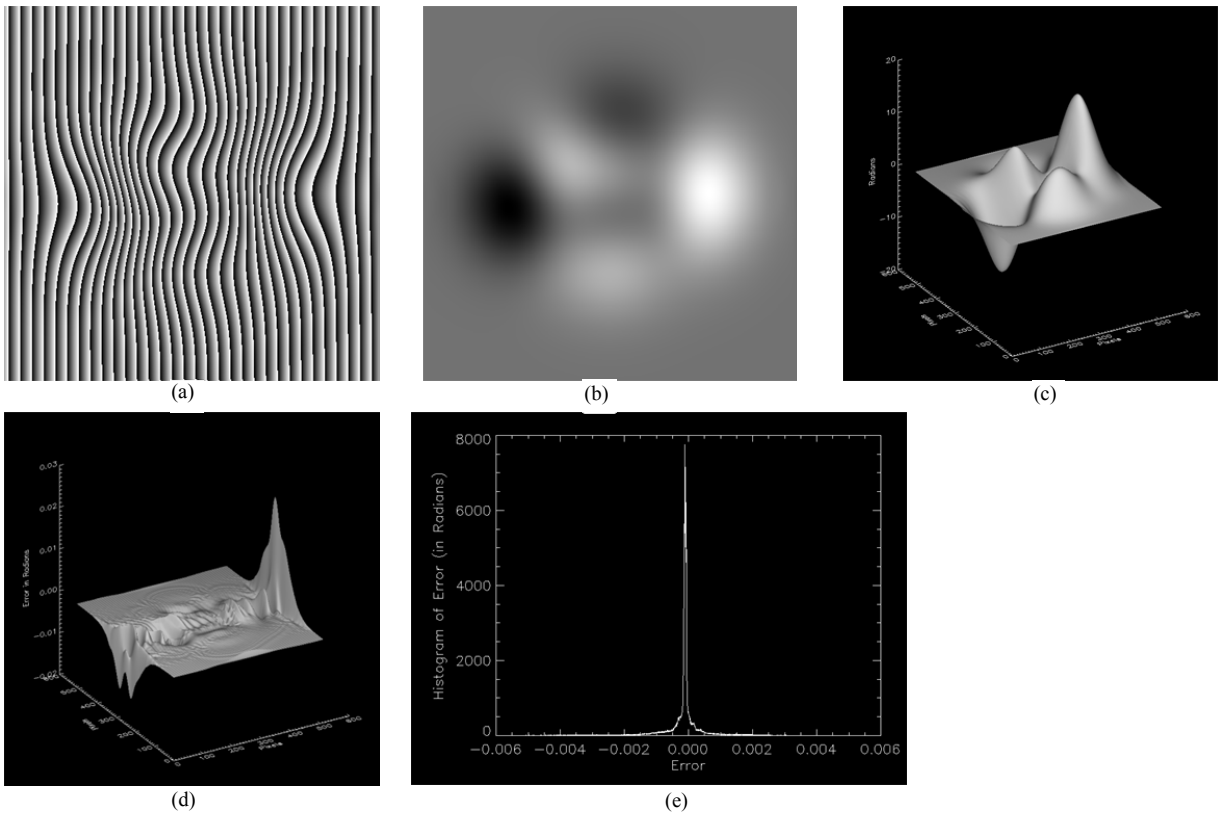

Figure 5: Errors produced by the Fourier transform method.

A white noise with a variance of 1 is added to the fringe pattern shown in Fig. 3c, which is equivalent to a signal to noise ratio of -3 dB. The resultant image is shown in Fig. 6a. This fringe pattern is processed using the 15-coefficient FIR filter. The produced wrapped phase map is shown in Fig. 6b, which is unwrapped using the basic phase unwrapped. The unwrapped phase is shown in Fig. 7c.

The noise performance of the 15-coefficient FIR filter algorithm is compared to the Fourier transform method as shown in Figs. 6d and 6e. The filtering in the frequency domain step in the Fourier transform method has been skipped for fair comparison between both algorithms. Both figures show that the FIR scheme slightly outperforms the Fourier transform method.

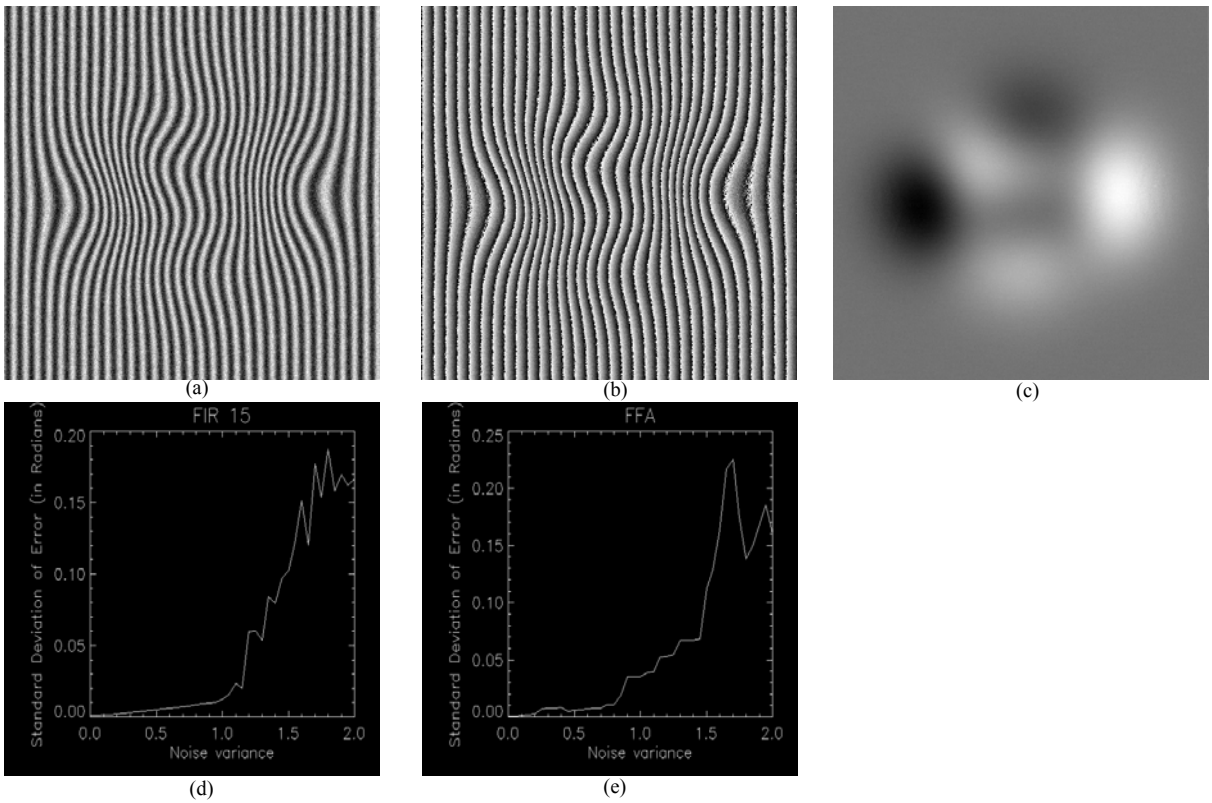

Figure 6: Noise performance of the 15-coefficent FIR and Fourier transform methods.

4. Experimental Results

The suggested algorithm was subsequently tested using real fringe patterns. Fig. 7a shows a real experimental fringe pattern image of a plaster cast of a human back illuminated with a structured lighting pattern, with the source fringe pattern image having a size of 512 × 512 pixels. This interferogram has been produced using a twin-fibre laser interferometer. The phase components in the interferogram are first extracted using the 15-coefficient FIR Hilbert transformer. The resultant wrapped phase map is shown in Fig. 7b and it is unwrapped using the basic phase unwrapper. The unwrapped phase map is shown in Figs. 7c and 7d.

The experiment was repeated using the Fourier transform method [6]. The resultant wrapped phase map is shown in Fig. 7e and it is unwrapped using the same basic phase unwrapper. The unwrapped phase map is shown in Figs. 7f and 7g. It is evident here that the phase produced using the Fourier transform method contains less noise than the phase produced using the FIR Hilbert transformer. This is due to the filtering of the noise in the frequency domain that is carried out by the Fourier transform technique.

The arithmetic difference between the unwrapped phase produced using the FIR Hilbert transformer and the Fourier transform methods was then calculated and plotted in 3D isometric form as shown in Fig. 7h. The standard deviation for this error is 0.0086 radians and the maximum value of the error is 0.19 radians, or approximately ($0.19/2\pi = 0.03$) of a fringe.

The whole experiment above is repeated for a second real fringe pattern, shown in Fig. 7i, that contains sudden phase changes and shadows. The fringe pattern is processed using the 15-coefficient FIR Hilbert transformer method and the extracted wrapped phase is shown in Fig. 7j. The wrapped phase is unwrapped using Flynn algorithm and the resultant phase map is shown in Figs. 7k and 7l [13]. This demonstrates the ability of the proposed method to cope with shadows and rapid phase changes.

For comparison purposes, the fringe pattern is processed using the Fourier transform method and resultant wrapped phase map is shown in Fig. 7m. The wrapped phase is unwrapped using Flynn algorithm and the resultant phase map is shown in Figs. 7n and 7o [13]. The arithmetic

difference between the unwrapped phase produced using the FIR Hilbert transformer and the Fourier transform methods was then calculated and plotted in 3D isometric form as shown in Fig. 7p.

Conclusion

This paper suggests the use of FIR Hilbert transformer to extract the phase of a fringe pattern image. This algorithm is significant in two respects. Firstly, it can be easily automated, as it does not rely upon the calibration of any of its parameters depending on the features of the specific fringe pattern that is being processed, neither is its implementation dependent upon the fringe projection system that is used to produce the fringe pattern. Secondly, this technique offers very fast execution times using digital computers. The paper introduces some promising initial results on both simulated and real data.

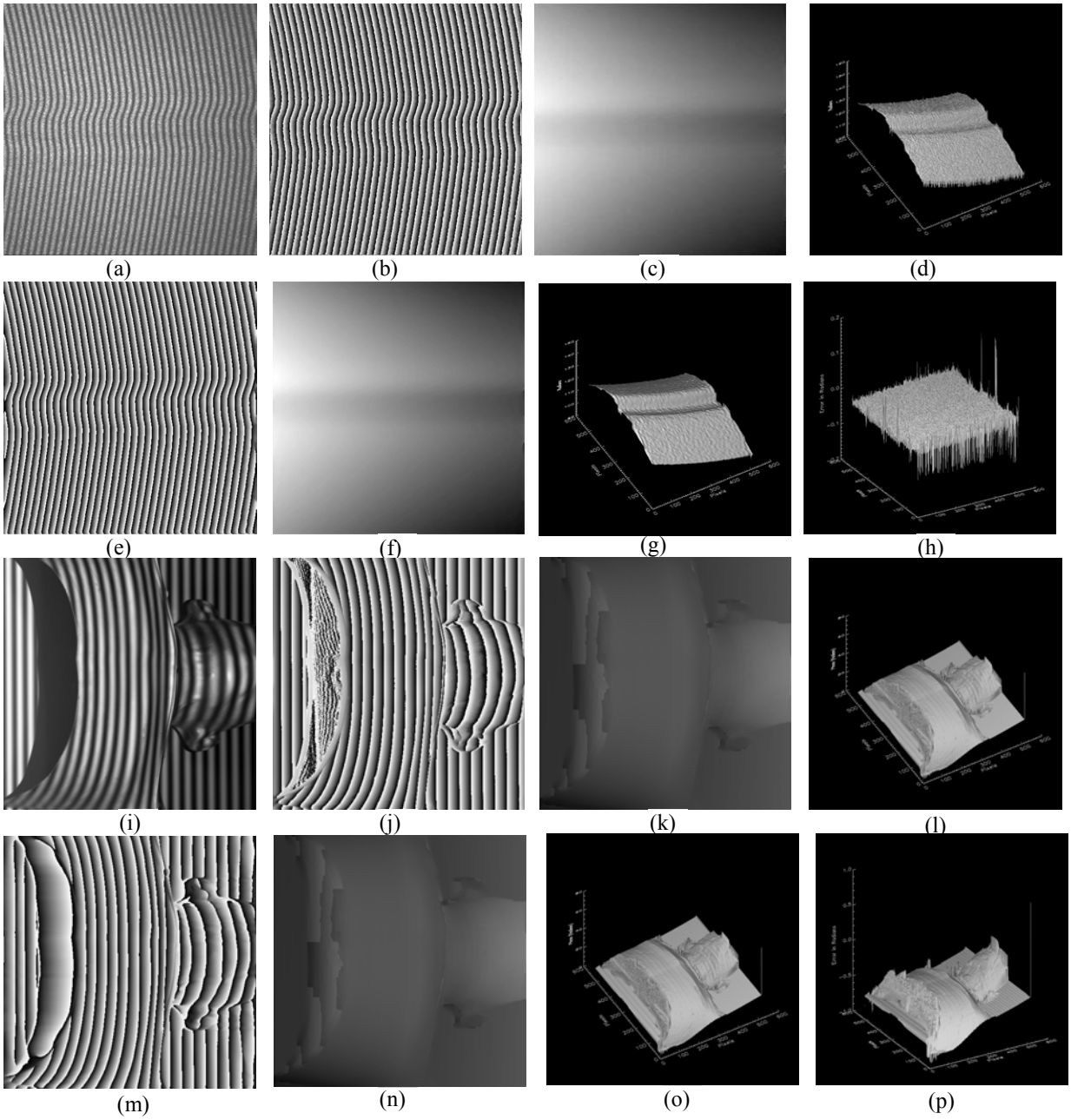

Figure 7: The process of the phase demodulation of a real fringe patterns using FIR Hilbert transformer and Fourier transform methods.

References

[1] P. Hariharan, in: W.R. Robinson, G. T. Reid (Eds.), Applications of interferogram analysis, Interferogram analysis: digital fringe pattern measurement techniques, Institute of Physics Publishing, Bristol and Philadelphia, 1993, pp. 262-284.

[2] K. Creath, in: W.R. Robinson, G. T. Reid (Eds.), Applications of interferogram analysis, Interferogram analysis: digital fringe pattern measurement techniques, Institute of Physics Publishing, Bristol and Philadelphia, 1993, pp. 94-140.

[3] Q. Zhang, Z. Hou, X. Wang, X. Li, Proc. SPIE 9276, Optical Metrology and Inspection for Industrial Applications III, 92760N (2014).

[4] M. A. Gdeisat, D. R. Burton, and M. J. Lalor, Applied Optics 45(2006) 8722-8732.

[5] Y. Qian, Y. Li, H. Wang, F. Hu, Optik 124 (2013) 456– 460.

[6] D. R. Burton, M. J. Lalor, Proc. SPIE 1163, Fringe Pattern Analysis 149 (1989).

[7] M. A. Gdeisat, A. Abid, D. R. Burton, M. J. Lalor, F. Lilley, C. Moore, M. Qudeisat, Optics and Lasers in Engineering 47(2009) 1348–1361.

[8] K. G. Larkin, J. Opt. Soc. Am. A 18 (2001) 1862-1870.

[9] L. Rabiner, R. Schafer, The Bell System Technical Journal 53 (1974) 363-390.

[10] L. Huang, Q. Kemao, B. Pan, A. K. Asundi, Optics and Lasers in Engineering (2009).

[11] D. Ghiglia, M. Pritt, Two-Dimensional Phase Unwrapping Theory, Algorithms and Applications, John Wiley & Sons (1998).

[12] EXELIS, http://www.exelisvis.com/ProductsServices/IDL.aspx. Accessed on 21st June 2015.

[13] T. J. Flynn, J. Opt. Soc. Am. A 14 (1997) 2692-2701.